Steel and Composite Structures, *Vol. 32, No. 5 (2019) 583-594*
DOI: https://doi.org/10.12989/scs.2019.32.5.583

Behavior of composite CFST beam-steel column joints

Soon-Sub Eom [1a], Quang-Viet Vu [1,2a], Ji-Hun Choi [1b],
George Papazafeiropoulos [3a] and Seung-Eock Kim [*1]

[1] *Department of Civil and Environmental Engineering, Sejong University, 98 Gunja-dong, Gwangjin-gu, Seoul, 05006, South Korea*
[2] *Faculty of Civil Engineering, Vietnam Maritime University, 484 Lach Tray Street, Ngo Quyen District, Hai Phong city, Vietnam*
[3] *Department of Structural Engineering, National Technical University of Athens, Zografou, Athens 15780, Greece*

(*Received February 24, 2019, Revised August 3, 2019, Accepted August 13, 2019*)

Abstract. In recent years, composite concrete-filled steel tubular (CFST) members have been widely utilized in framed building structures like beams, columns, and beam-columns since they have significant advantages such as reducing construction time, improving the seismic performance, and possessing high ductility, strength, and energy absorbing capacity. This paper presents a new composite joint - the composite CFST beam-column joint in which the CFST member is used as the beam. The main components of the proposed composite joint are steel H-beams, CFST beams welded with the steel H-column, and a reinforced concrete slab. The steel H-beams and CFST beams are connected with the concrete slab using shear connectors to ensure composite action between them. The structural performance of the proposed composite joint was evaluated through an experimental investigation. A three-dimensional (3D) finite element (FE) model was developed to simulate this composite joint using the ABAQUS/Explicit software, and the accuracy of the FE model was verified with the relevant experimental results. In addition, a number of parametric studies were made to examine the effects of the steel box beam thickness, concrete compressive strength, steel yield strength, and reinforcement ratio in the concrete slab on the proposed joint performance.

Keywords: concrete-filled steel tubular; composite joints; finite element model; ABAQUS/explicit

1. Introduction

CFST members consisting of a steel hollow section and concrete infill utilize the advantages of both concrete and steel. The use of CFST members can decrease the construction time and enhance the seismic performance since they possess high stiffness, high strength, ductility, and large energy absorption. Therefore, in recent years, they have been extensively employed in low-rise buildings as beams and in high-rise buildings as columns and beam-columns (Han *et al*. 2004, 2010, Tao and Han 2006, Moon *et al*. 2012, Esfandyary *et al*. 2015, Hassan *et al*. 2016, Thomas and Sandeep 2018, Yuan *et al*. 2019, Eom *et al*. 2019). The use of CFST columns in beam-to-CFST column joints has been considered extensively in the literature through experimental tests, finite element analyses (FEA) and analytical approaches (Elremaily and Azizinamini 2001, Wang *et al*. 2009a, b, Hassan *et al*. 2014, Yang *et al*. 2015, Li *et al*. 2018). Wang *et al.* (2009a) conducted an experimental study involving bolted moment connection joints of square or circular CFST columns, and steel-H beams using high-strength blind bolts subjected to monotonic loading, while the experimental investigation by Yang *et al.* (2015) examined the rotation behavior of a simply bolted I-beam to concrete-filled elliptical steel tubular column joints. By performing experimental and numerical analysis, Wang *et al.* (2009b) investigated the mechanical behavior of blind bolted end plate joints to concrete-filled thin-walled steel tubular columns, proposing an innovative blind bolted joint that could be applied in low-rise and mid-rise buildings. More recent works on composite beam-to-CFST column joints have been widely undertaken (Loh *et al*. 2006, Ataei *et al*. 2015, 2016a, b, c, 2017, Thai and Uy 2015, Ataei and Bradford 2016, Thai *et al*. 2017, Wang *et al*. 2018, Waqas *et al*. 2019). Among these, experimental studies of the flush end plate and high strength steel flush end plate beam-to-column composite joints with deconstructable bolted shear connectors have been conducted (Ataei *et al.* 2015, 2016a). The proposed composite joint could be easily deconstructed at the end of its service life, and the demolition waste is minimized and the recycling of its components is maximized. The results also suggest the use of precast slabs in the composite joint to enhance the quality of construction, decrease the construction time and labor costs. An experimental study by Thai *et al.* (2017) examined the structural performance of blind bolted end plate composite joints to the square and circular CFST columns and an analytical model to predict the moment-rotation behavior of the composite joint was proposed. By performing experimental and numerical studies, Waqas *et al*. (2019) investigated the response of composite beam-to-CFST column flush end plate connections using blind bolts subjected to static and cyclic loading. The experimental results proved that strength and

*Corresponding author, Professor,
E-mail: Sekim@sejong.ac.kr
[a] Ph.D. Student
[b] M.S. Student

ISSN: 1229-9367 (Print), 1598-6233 (Online)

Table 1 Details of the specimen

No	Member	Dimensions(mm)
1	Steel column	H 350×350×12 mm
2	Concrete slab	5200×2675×160 mm
3	Steel box beam	390×350×10 mm
4	Concrete filled steel tubular beam	362×330×2185 mm
5	Headed shear studs	M25×100 mm
6	Longitudinal reinforcing bars	N16
7	Transverse reinforcing bars	N19
8	Diagonal reinforcing bars	N19
9	Steel H-beam	H 390×300×10 mm
10	End plate	390×350×20

stiffness are enhanced compared to previous works.

As stated above, CFST members can be used in the buildings as columns, beams, and beam-columns. Extensive research related to the composite beam-to-CFST column joints using experimental and numerical approaches has been implemented; however, to the best of the authors' knowledge, no research on the composite CFST beam-to-column joints has been made so far. In addition, generally steel H-beam has been used only for conventional welded joints (Yang and Kim 2007, Jordão *et al*. 2014, Tong *et al*. 2016) and not for CFST beams that can enhance the capacity of the joint.

This paper aims at introducing and investigating the behavior of a new joint namely the composite CFST beam-column joint. An experimental investigation was conducted to evaluate the structural performance of this composite joint subjected to static loading. A 3D FE model was developed to simulate this composite joint using the commercial software ABAQUS/Explicit. Parametric studies were performed to estimate the effect of the thickness of steel box beam, the concrete compressive strength, and the yield strength of steel and reinforcement ratio in the concrete slab on the proposed composite joint behavior.

2. Experimental program

2.1 Specimen design

The proposed composite joint was designed in accordance with KBC 2016 (2016), KSCDC 2012 (2012), and KDS 14 31 10:2017 (2017). Details are shown in Fig. 1 and summarized in Table 1.

The main components of the composite joint include the steel H-column, CFST beams, steel H-beam and reinforced concrete slab. The steel H-column is comprised of a rolled steel section, while the steel H-beam has a built-up section. The CFST beam is comprised of a rectangular shaped steel hollow section filled with plain concrete. For the reinforced concrete slab, the main reinforcement consists of 14N16 steel bars which are placed along the longitudinal direction, whilst 42N19 bars are distributed along the transverse direction in two layers. Moreover, N19 diagonal bars are located at the connection between the column and the CFST beams in order to avoid stress concentration effects. It is noted from Fig. 1 that two splices were used for more convenient transportation of the components and construction of the composite joint. The CFST beams were directly welded with the steel H-column, whilst the steel H-beams were connected with the CFST beams using end plates. The specimen was constructed so that it represents as much as possible a joint in a real framed structure, in which the CFST beams are placed at the negative moment regions, and the steel H-beams are located at the positive moment regions. This arrangement aims to enhance the ultimate strength at the negative moment region and save the material at the positive moment region of the framed structure. In addition, both the CFST beams and the steel-H beams are connected to the reinforced concrete slab using M25 shear connectors to provide full composite action between them. The specimen along with the whole experimental set up are shown in Fig. 2.

Table 2 Material properties for steel and concrete

No	Type of steel	Thickness/ Diameter	Yield strength F_y (MPa)	Ultimate strength, F_u (MPa)	Elastic modunlus, E_s (MPa)	Elongation (%)
1	Steel column (Flanges and web)	19 and 12 mm	440	569	200,000	26.5
2	Flanges of steel box beam	14 mm	421	560	200,000	24
3	Web of steel box beam	10 mm	405.4	554.6	200,000	24
4	Longitudinal reinforcing bars	D16	547	670	200,000	16.3
5	Transverse reinforcing bars/ Diagonal reinforcing bars	D19	545	671	200,000	15.4
6	Flanges of steel H-beam	16 mm	407	540	200,000	27
7	Web of steel H-beam	10 mm	405.4	554.6	200,000	24
8	End plate	20 mm	359	544	200,000	25

No	Specimen	Compressive strength, f_{ck} (MPa)	Compressive strain, ε_c	Tensile strength, f_{tk} (MPa)	Tensile displacement, (mm)
1	Concrete slab/Concrete filled steel tubular beam	40.45	0.0028	3.89	1 mm

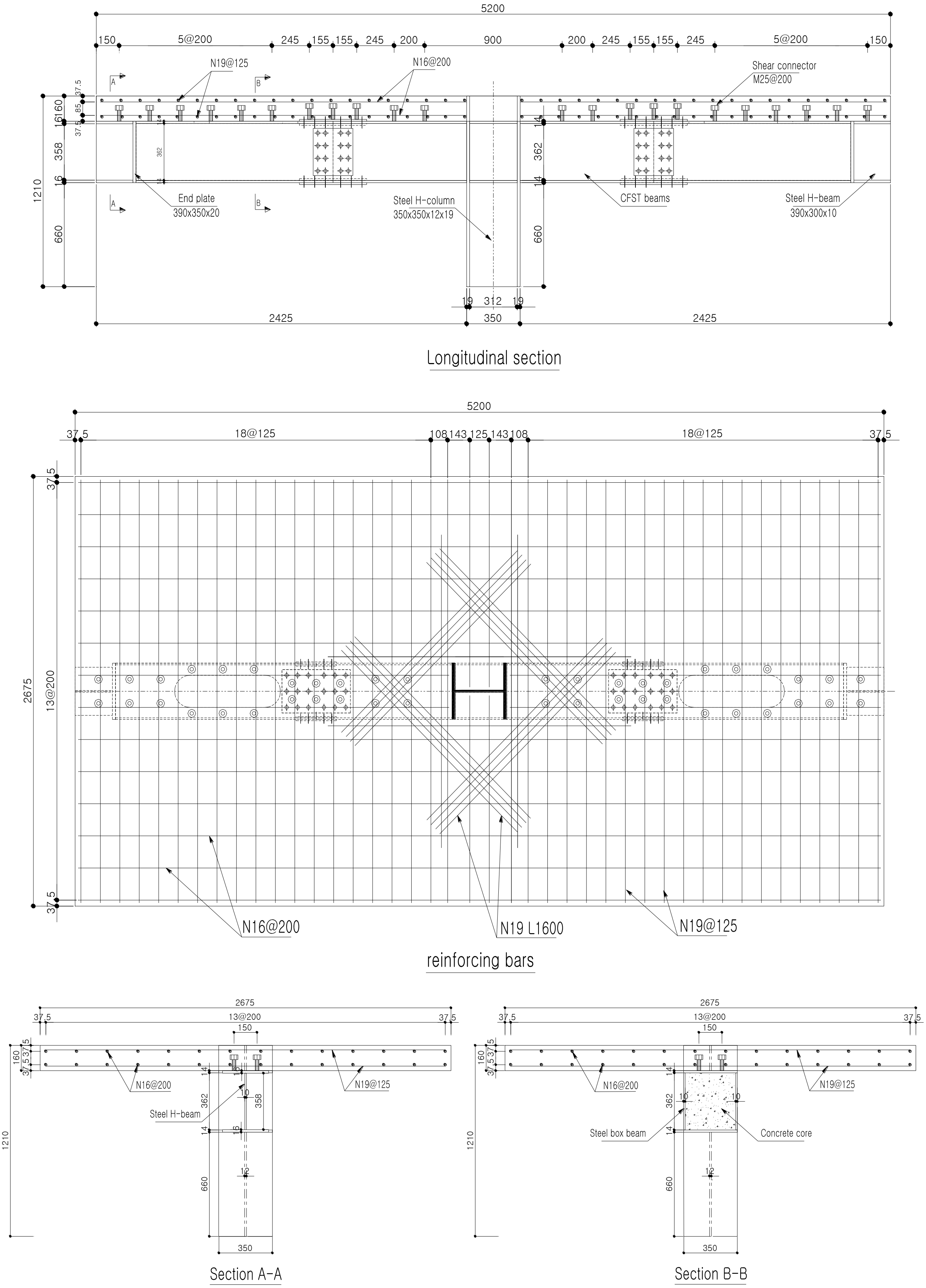

Fig. 1 Detailed geometry of specimen

Fig. 2 Specimen preparation

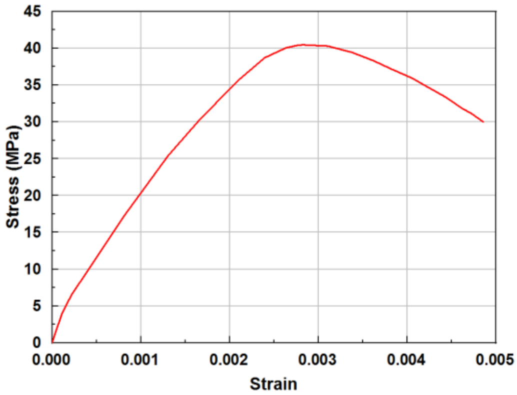

Fig. 3 Stress-strain relationship of concrete cylinder

Fig. 4 Test set-up

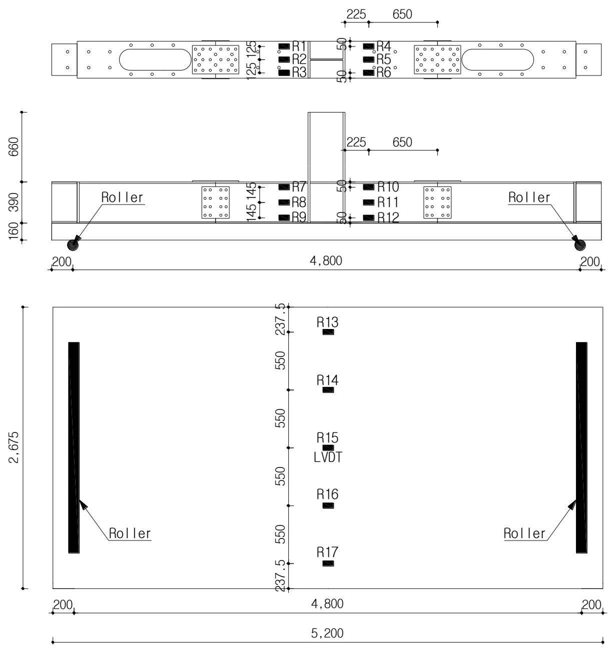

Fig. 5 Instrumentation layout

2.2 Material properties

SM490 steel plates were used for the steel box beam, steel column, steel H-beam, and end plate, while SD500 steels were used for reinforcing bars in the slab of the composite joint. Tensile coupon tests were performed using a displacement controlled testing machine to obtain the material properties of all the structural steel components according to the Korean Standard KS D 3515:2014 (2014). Cylinder compression tests were undertaken based on Korean Standard KS F 2405 (2010) to determine the concrete compressive strength at 28 days after casting while splitting cylinder tests were used to identify the indirect concrete tensile strength. All the material properties are demonstrated in Table 2 and Fig. 3.

2.3 Experimental setup

The test set-up for the composite joint is shown in Fig. 4. The joint was loaded vertically at the top of steel column

(a) Deformation of the specimen

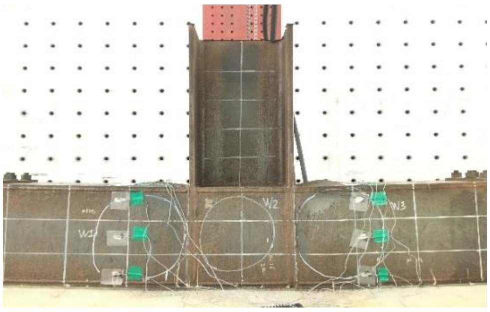

(b) Local buckling of the steel box beam

(c) Crack pattern in concrete slab

Fig. 6 Failure mode of the specimen

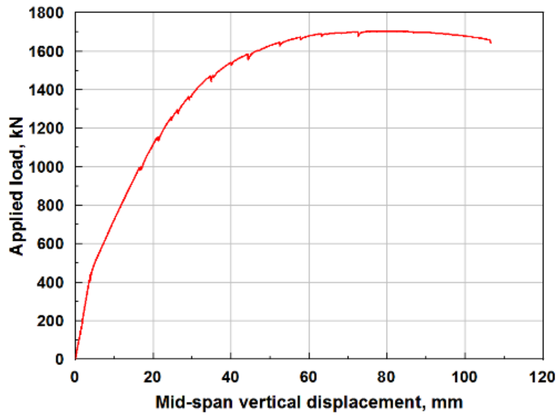

Fig. 7 Load – displacement response of the specimen

using a hydraulic jack with a loading capacity of 5 MN. Before performing the test, a small load of about 10% of the predicted ultimate load of the specimen was imposed to check the set-up and performance of the components and instrumentation. The specimen was unloaded and reloaded, and the deformation was monotonically raised until no further loading can be sustained by the specimen. The test was displacement-controlled using a loading rate of 2 mm/min. Various measurement devices consisting of strain gauges and Linear Variable Displacement Transducer (LVDT) were used to measure respectively the strain and displacement at different positions of the specimen and to assess the structural performance and the behavior of the composite joint. The arrangement of the measurement instruments at the specimen is illustrated in Fig. 5.

2.4 Experimental results

Fig. 6 shows the typical failure mode, while Fig. 7 presents the applied load versus displacement response of the composite joint. The ultimate load and the corresponding moment capacity of this joint are 1705 kN and 1939.44 kN.m respectively. It can be observed that the specimen failed in a ductile manner because it was able to sustain remarkable deformation at the ultimate load. After the yielding of the steel box beam, the test was stopped since local buckling occurred at this beam near the steel H-column, as illustrated in Fig. 6(b). At a load of 170 kN, the first crack happened at around the mid-span of the specimen. At the end of the test, cracks occurred around the steel column surface and propagated towards concrete slab edges following an inclined pattern, as presented in Fig. 6(c).

Fig. 8 depicts the load-strain responses in the top and lateral faces of the steel box beam and in the bottom of the concrete slab of the specimen. It can be observed that the strains in the top face are greater than those in the lateral face of the steel box beam. It is also worth noting from Figs. 8a and 8b that the strains in the steel box beam significantly exceeded the yield strain achieved from the result of tensile tests. Apparently, yielding of webs and flanges of the steel box beam occured.

3. Finite element analysis

The commercially available software, ABAQUS (2014), was used to model the composite CFST beam – steel column joint. A 3D FE model was developed to examine the behavior of this joint. Since the contacts used in this joint were complex, the explicit method was adopted to avoid numerical convergence difficulties and reduce the running time. Fig. 9 provides a general layout of the FE model.

3.1 Element type and mesh

To reduce the computational time and cost, and obtain reliable results, suitable element types should be selected for the FE model. In the current study, 3D eight-node reduced integration solid elements (C3D8R) were employed to simulate the concrete slab and concrete infill in the steel box beam. Four-node reduced integration shell elements (S4R) were employed for the modeling of the steel box beam, steel H-beam, and steel H-column since this element type is the most appropriate for thin-walled steel structures.

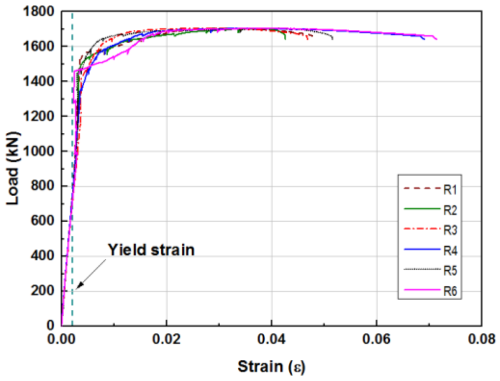

(a) Top face of the steel beam

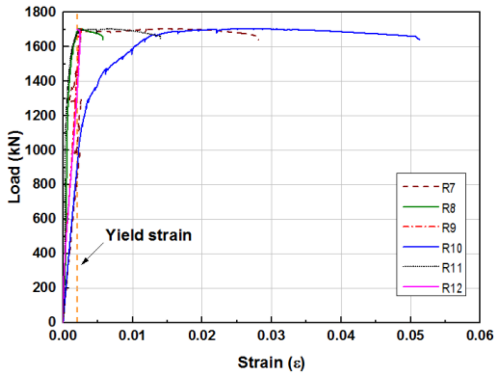

(b) Lateral face of the steel beam

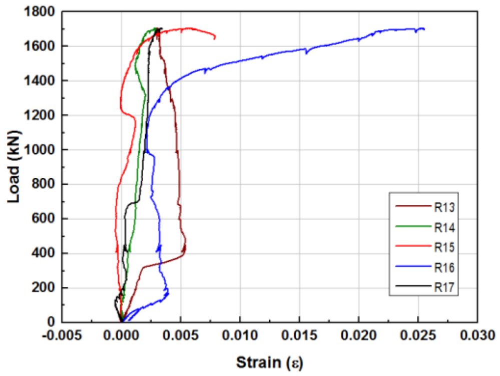

(c) Bottom of the slab

Fig. 8 Load-strain response at various locations of the specimen

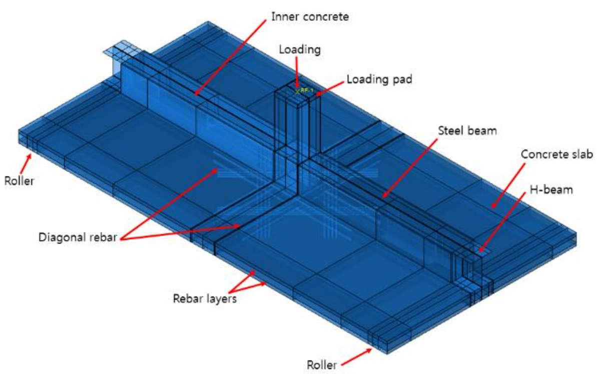

Fig. 9 General layout of the FE model of the composite joint

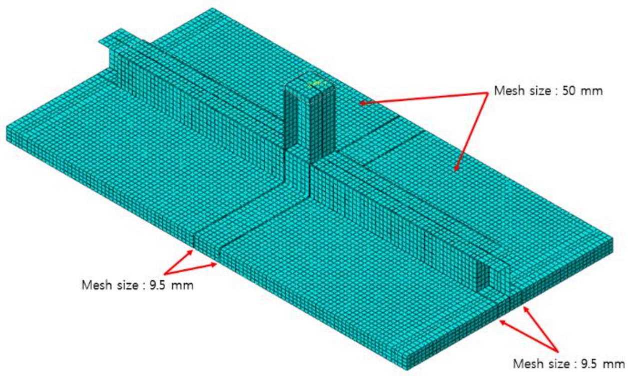

Fig. 10 FE mesh of the composite joint

For reinforcement in the concrete slab four-node quadrilateral surface elements (SFM3D4) were utilized to simulate longitudinal and transverse reinforcements using the REBAR option, while three-dimensional truss elements (T3D2) were used to model the diagonal reinforcement. Finally, rigid elements (R3D4) were applied for modeling the loading pad.

Sensitivity analysis was conducted to find an acceptable mesh refinement to ensure that the model provides reliable results. Results from preliminary analyses revealed that a mesh size of 50 mm was reasonable, and this was used for all case studies. Fig. 10 shows the FE mesh adopted for the composite joint.

3.2 Material models

For the concrete model, the concrete damaged plasticity (CDP) model available in ABAQUS was employed for the concrete slab and the concrete infill, which can capture both the cracking and crushing failures of the concrete. The stress-strain curve indicated in Fig. 3 was used to model the concrete in compression. Regarding the concrete in tension, the stress-displacement curve was utilized to model the brittle response of the concrete instead of the stress-strain relationship. The concrete tensile model adopted by Kim and Nguyen (2010, 2012) was employed. Fig. 11 illustrates the stress-displacement response of the concrete in tension based on the cubic Bézier curve with actual crack opening of 1 mm. The tensile damage model was considered based on Kim and Nguyen (2010, 2012), while the compressive damage was not taken into consideration because the failure mode obtained from the test was due to concrete cracking.

For the steel model, the bi-linear stress-strain relationship was utilized as demonstrated in Fig. 12. The yield strength F_y, yield strain ε_y, ultimate strength F_u, and the ultimate strain ε_u were obtained from tensile test results.

3.3 Contact and constraint conditions

The general contact algorithm was employed in modeling the contact interaction between various components of the composite joint. In this analysis, general contact was applied for the contact between concrete and steel with a friction coefficient of 0.1 and a hard contact formulation. Two contact pairs were defined in the model:

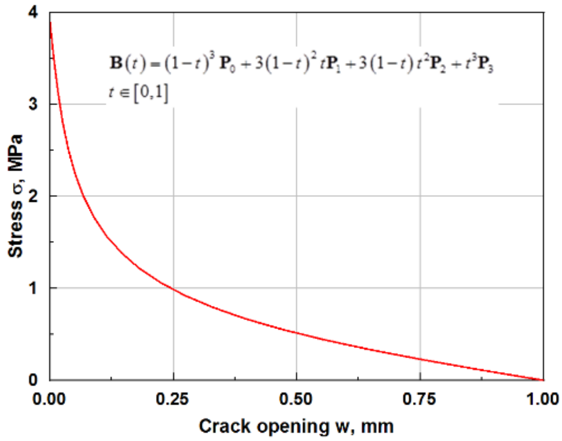

Fig. 11 Tension stiffening model based on the cubic Bézier curve

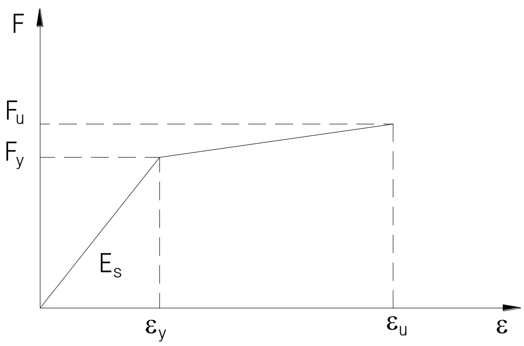

Fig. 12 General stress-strain relationship of steel material used in this study

(1) steel column and concrete slab, and (2) concrete infill and steel box beam.

Embedded constraints were utilized to simulate the interaction between the concrete slab and the reinforcing bars. In this constraint, the bars play the role of an embedded region and the slab plays the role of a host region. This technique simulates the contact between the reinforcing bars and the concrete slab as a perfect bond. On the other hand, tie constraint was utilized to model the interaction between the loading pad and the steel column. In the experimental test, any slip that may exist between the concrete slabs and the CFST beams has not been monitored, since this is out of the scope of the present study. Therefore, the shear connectors have not been modeled in detail in the finite element model considered in this study but a surface – to – surface tied connection has been used instead between the corresponding steel beam and the concrete slab interfaces as is done in the paper of Vu *et al.* (2018).

It is noted that all the components, i.e., steel H-beams, end plate, steel box beams, and steel H-column, were assembled together. In addition, the presence of the splices which contain the cleats is not taken into account in the FE model since in the experimental setup, the splices are designed to satisfy the strength requirements in the related standards. Therefore, they do not affect the response of the CFST beam-column joint at failure.

Table 3 Details of the specimen

Model	Ultimate load (kN)	Difference (%)	Displacement (mm)	Difference (%)
Test	1704.70		106.56	
FEA	1710.26	0.33	107.82	1.18

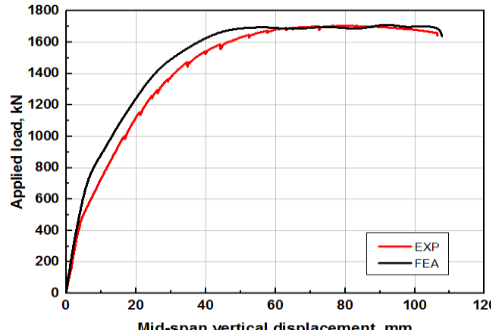

Fig. 13 Comparison of load-displacement curves between FEA and experimental results

3.4 Loading and boundary conditions

On the lower face of the concrete slab at both ends, the simply supported boundary condition was imposed based on the test set-up. The vertical applied load was imposed on the structure through the reference point placed at the top center of the loading pad using the displacement control method. A loading rate equal to 2 mm/min utilized in the actual test was applied in the model using the smooth step amplitude available in Abaqus/Explicit.

3.5 Model verification

The accuracy of the developed FE model is validated by comparing the FE results with the experimental results reported in Section 2. Fig. 13 indicates the comparison of load-displacement curves, while Table 3 presents the comparison of the ultimate load and mid-span displacement between FEA and experimental results with a good agreement observed.

As illustrated in Fig. 14, the developed FE model can also accurately predict the failure mode of the composite joint since the failure modes obtained from the experiment and from the analysis results are almost similar. Thus, it is concluded that the developed FE model is accurate and can capture the real behavior of the composite CFST beam-steel column joint.

4. Parametric studies

The FE model verified by the test result was employed to conduct a number of parametric studies to investigate the influence of various parameters on the response of the composite CFST beam-to-steel column joint. In the parametric studies, results which show the steel box beam thickness effect, the concrete compressive strength effect,

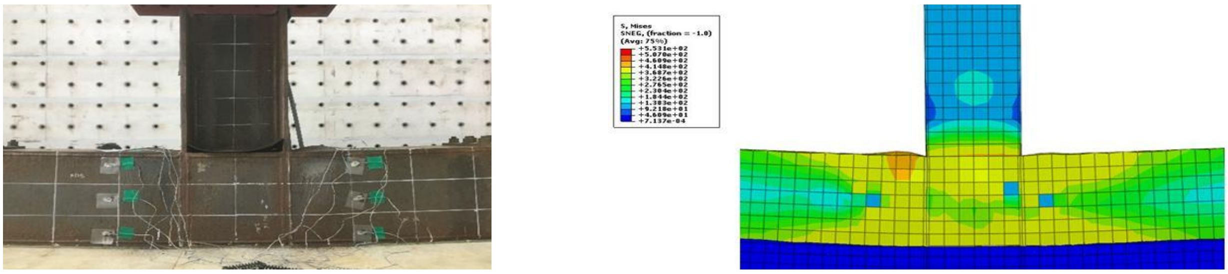

(a) Plastic strain and local buckling of the flange and web of steel box beam

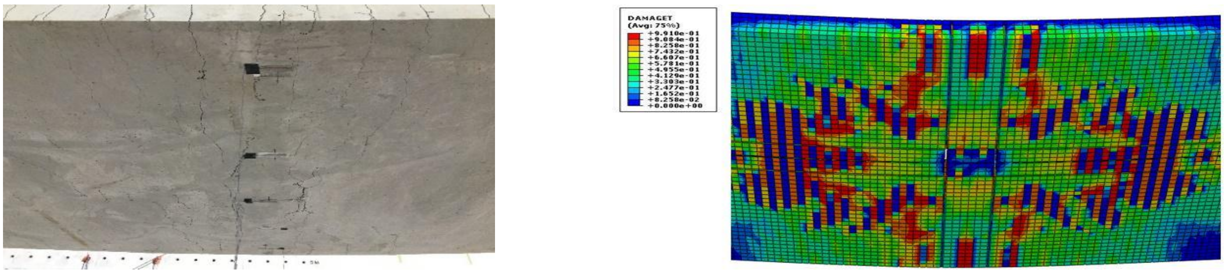

(b) Crack of concrete slab

Fig. 14 Comparison of failure modes between FEA and experimental results

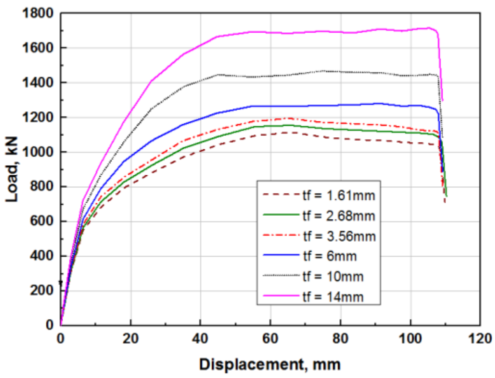

Fig. 15 Load-displacement response of the composite joint for various flange thicknesses of the steel box beams

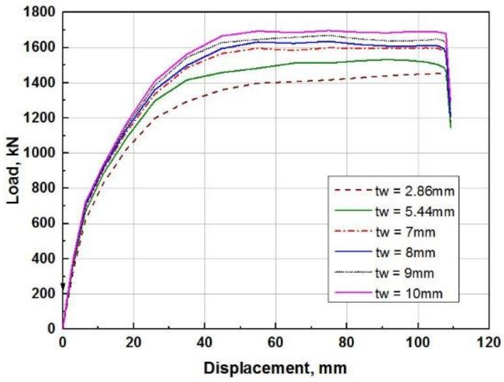

Fig. 16 Load-displacement response of the composite joint for various web thicknesses of the steel box beams

the steel yield strength effect, and the reinforcement ratio effect are presented in Table 4. The results in the following sections are presented in terms of load-displacement curves and not of moment-rotation curves, since the rotation of plastic hinges is generally hard to estimate because of the real-time changes in their length and the difficulties in decoupling the composite action between the CFST beams and the slab, as well as between the two beams that share the composite joint with the steel H-column.

4.1 Effect of flange thickness of steel box beam

To examine the influence of the flange thickness of the steel box beam, various flange thicknesses were considered in Group 1 as provided in Table 4. The thicknesses of 1.61, 2.68, and 3.56 mm are the minimum values for the slender, non-compact, and compact flanges of the steel box, respectively, which are calculated based on the requirement of the KSCDC 2012 (2012). However, in the case with the minimum flange thickness of the steel box beam, it may be practically difficult to deploy shear connectors between the steel box beam and the slab; anyway this case is considered here since it is acceptable by the norm. Fig. 15 depicts the load-displacement curves corresponding to various flange thicknesses. It can be seen from this figure that there is a slight difference in ultimate loads of the composite joints with steel box beams having the minimum flange thicknesses to satisfy slender, non-compact and compact flanges. However, for the specimens with steel boxes having compact flanges, the flange thickness significantly affects the ultimate strength. In Fig. 15, it appears that the percentages of increase in the ultimate loads computed are 7.18%, 22.82%, and 43.53% by changing the flange thickness from 3.56 mm to 6, 10, and 14 mm, respectively.

4.2 Effect of web thickness of steel box beam

The effects of the web thickness of the steel box beam on the behavior of the composite joint were also examined by varying the web thicknesses as found in Group 2 in

Table 4 Geometric and material properties of composite CFST beam-to-steel column joint used in the parametric study

Group	Composite joint	b_{sbb} x tf (mm)	h_{sbb} x tw (mm)	f'_{c1} (MPa)	f'_{c2} (MPa)	F_y (steel beam) (MPa)	Reinforcement ratio	Reinforcement spacing (mm)
1	CJ-1	350 × 1.61	362 × 10	40.45	40.45	421 (560)	14N16	200
	CJ-2	350 × 2.68	362 × 10	40.45	40.45	421 (560)	14N16	200
	CJ-3	350 × 3.56	362 × 10	40.45	40.45	421 (560)	14N16	200
	CJ-4	350 × 6	362 × 10	40.45	40.45	421 (560)	14N16	200
	CJ-5	350 × 10	362 × 10	40.45	40.45	421 (560)	14N16	200
2	CJ-7	350 × 14	362 × 2.86	40.45	40.45	421 (560)	14N16	200
	CJ-8	350 × 14	362 × 5.44	40.45	40.45	421 (560)	14N16	200
	CJ-9	350 × 14	362 × 7	40.45	40.45	421 (560)	14N16	200
	CJ-10	350 × 14	362 × 8	40.45	40.45	421 (560)	14N16	200
	CJ-11	350 × 14	362 × 9	40.45	40.45	421 (560)	14N16	200
3	CJ-12	350 × 14	362 × 10	30	40	421 (560)	14N16	200
	CJ-13	350 × 14	362 × 10	40	40	421 (560)	14N16	200
	CJ-14	350 × 14	362 × 10	50	40	421 (560)	14N16	200
	CJ-15	350 × 14	362 × 10	60	40	421 (560)	14N16	200
	CJ-16	350 × 14	362 × 10	70	40	421 (560)	14N16	200
	CJ-17	350 × 14	362 × 10	80	40	421 (560)	14N16	200
4	CJ-18	350 × 14	362 × 10	40	30	421 (560)	14N16	200
	CJ-19	350 × 14	362 × 10	40	50	421 (560)	14N16	200
	CJ-20	350 × 14	362 × 10	40	60	421 (560)	14N16	200
	CJ-21	350 × 14	362 × 10	40	70	421 (560)	14N16	200
	CJ-22	350 × 14	362 × 10	40	80	421 (560)	14N16	200
5	CJ-23	350 × 14	362 × 10	40.45	40.45	235 (340)	14N16	200
	CJ-24	350 × 14	362 × 10	40.45	40.45	275 (410)	14N16	200
	CJ-25	350 × 14	362 × 10	40.45	40.45	355 (490)	14N16	200
6	CJ-26	350 × 14	362 × 10	40.45	40.45	421 (560)	14N13	200
	CJ-27	350 × 14	362 × 10	40.45	40.45	421 (560)	14N16	200
	CJ-28	350 × 14	362 × 10	40.45	40.45	421 (560)	14N19	200
	CJ-29	350 × 14	362 × 10	40.45	40.45	421 (560)	14N22	200
	CJ-30	350 × 14	362 × 10	40.45	40.45	421 (560)	14N25	200
	CJ-31	350 × 14	362 × 10	40.45	40.45	421 (560)	14N29	200

Table 4. The minimum thicknesses for the non-compact and compact webs of the steel box are 2.86 and 5.44 mm, respectively. The load-displacement responses for various web thicknesses are indicated in Fig. 16. It is noted that the influence of the steel box web thickness on the ultimate strength of the composite joint is small, especially for the specimens whose the web thickness of the steel box beam is higher than 7 mm. The maximum difference in the ultimate load of the specimen is only 5.5% calculated between the cases of the steel box beam having non-compact and compact webs.

4.3 Effect of concrete compressive strength

In this section, the influence of the compressive strengths of concrete infill and concrete slab on the response of the composite joint are investigated. The concrete compressive strength is varied from 30 to 80MPa as shown in Groups 3 and 4 in Table 4. The stress-strain relationship of the concrete in compression corresponding to various compressive strengths is determined based on EC2 (Eurocode 2 2004).

4.3.1 Effect of compressive strength of concrete slab

To identify the effect of compressive strength of the concrete slab on the response of the composite joint, the compressive strength of concrete infill was fixed at 40 MPa and the compressive strength of concrete slab was varied from 30 to 80 MPa. Fig. 17 reveals the load-displacement responses for various compressive strengths of the concrete slab. It is deduced from the results that the compressive

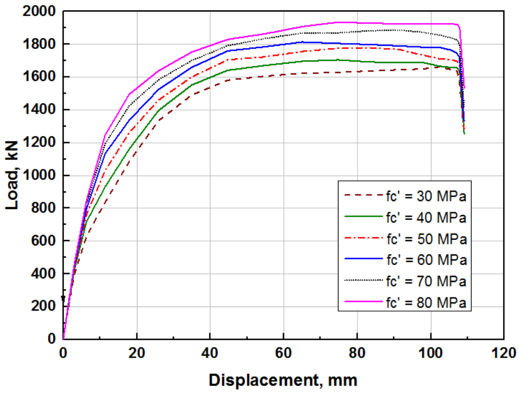

Fig. 17 Load-displacement response of the composite joint for different compressive strengths of concrete slab

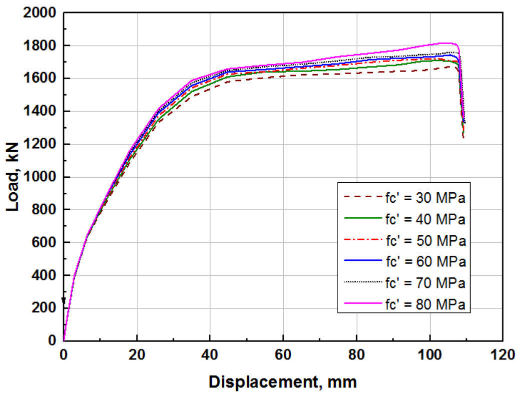

Fig. 18 Load-displacement response for the composite joint for different compressive strengths of concrete infill

strength of the concrete slab does have a remarkable effect on the ultimate strength of the composite joint. A probable reason for which the ultimate resistance increases along with an increase in the compressive strength of concrete slab is that the plastic neutral axis lies in the concrete slab when the load is applied.

4.3.2 Effect of compressive strength of concrete infill

To examine the influence of the compressive strength of concrete infill on the response of the composite joint, the compressive strength of concrete slab was fixed at 40 MPa, while the compressive strength of the concrete infill was changed from 30 to 80 MPa. Fig. 18 illustrates the comparison of the load-displacement response with the different compressive strengths of the concrete infill. From this figure, only a slight influence of the concrete infill on the ultimate strength of the composite joint is detected.

4.4 Effect of yield strength of steel

The effect of the yield strength of the steel box beam on the performance of the composite joint in Group 5 presented in Table 4 was investigated. The yield strengths

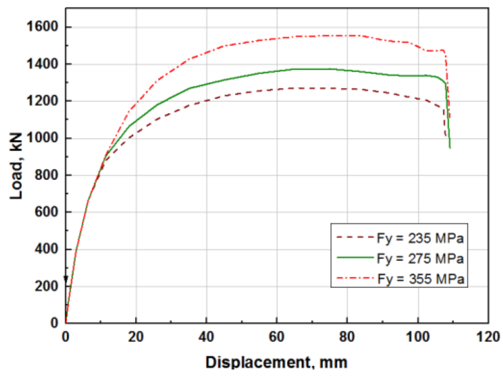

Fig. 19 Load-displacement response of the composite joint for different yield strengths of steel beam

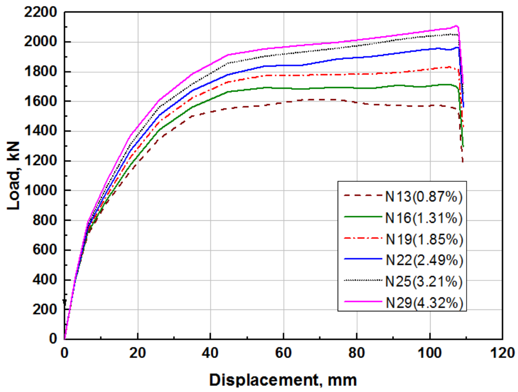

Fig. 20 Load-displacement response for the composite joint for different reinforcement ratios in the concrete slab

of the steel-H column and steel-H beam were fixed, and only the yield strengths of the steel box beam varied from 235 to 375 MPa. The load-displacement curves for the various steel box yield strengths are illustrated in Fig. 19. It is observed from this figure that the yield strength of steel beam does not have any influence on the initial stiffness of the joint but at higher loads, steel beams with higher yield strengths exhibit higher stiffness. Increasing the yield strength of steel beams leads to an increase in the ultimate strength of the composite joint. When the yield strength of steel beams increases from 235 MPa to 275 and 355 MPa, the ultimate strength of the composite joint increases by 8.17% and 13.10%, respectively.

4.5 Effect of reinforcement ratio

Fig. 20 presents the effect of the reinforcement ratio on the load-displacement curves of the composite joint. Six different reinforcement diameters of N13, N16, N19, N22, N25, and N29 corresponding to reinforcement ratios equal to 0.87, 1.31, 1.85, 2.49, 3.21, and 4.32% respectively were taken into consideration in the parametric study. Fig. 20 indicates that there is a remarkable influence of the reinforcement ratio on the ultimate strength of the composite joint. When the reinforcement ratio increases (up to about 3.2%), the ultimate load of the composite joint

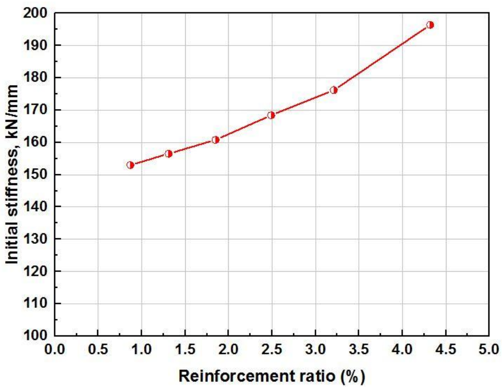

Fig. 21 Variation of initial stiffness with respect to reinforcement ratio in the slab

significantly increases. However, the strength of the joint only slightly increases when the reinforcement ratio exceeds 3.2%.

Fig. 21 shows the variation of the initial stiffness with respect to reinforcement ratio in the concrete slab. It is observed that there is a slight increase in the initial stiffness of beam-to-column joints with increasing reinforcement ratio in accordance with other analogous results that have been published in the literature (e.g., Ataei and Bradford 2016, Ataei *et al*. 2016b, 2017).

5. Conclusions

In this study, a composite CFST beam-steel column joint, has been studied both experimentally and numerically. The behavior of this composite joint has been investigated for various values of the design parameters. The following conclusions have been drawn:

- The developed FE model can accurately predict the behavior of the composite CFST beam-steel column joint.
- The flange thickness of steel box beam has a remarkable effect on the ultimate strength of the composite joint with steel boxes having compact flanges, but not for the joint with steel boxes having the minimum thicknesses to satisfy the slender, non-compact, and compact flanges.
- The web thickness of the steel box beam has a minor effect on the ultimate strength of the composite joint when it is larger than 7 mm.
- The use of higher strength steel beams in a composite joint leads to higher ultimate strength of the joint.
- The compressive strengths of the concrete slab and concrete infill do not have any remarkable influence on the ultimate strength of the composite joint.
- Increasing the reinforcing ratio to a certain value can significantly increase the load carrying capacity of the composite joint. However, further increase in this ratio above this value will only have a slight effect on the ultimate strength of the joint.

Acknowledgments

This work was supported by the National Research Foundation of Korea (NRF) grant funded by the Korea government (MSIT) (No. 2018R1A2A2A05018524).

References

ABAQUS (2014), Analysis user’s manual version 6.14, Dassault Systems.

Ataei, A., Bradford, M.A. and Valipour, H.R. (2015), “Experimental study of flush end plate beam-to-CFST column composite joints with deconstructable bolted shear connectors”, *Eng. Struct*., **99**, 616-630. https://doi.org/10.1016/j.engstruct.2015.05.012

Ataei, A., Bradford, M.A., Valipour, H.R. and Liu, X. (2016a), “Experimental study of sustainable high strength steel flush end plate beam-to-column composite joints with deconstructable bolted shear connectors”, *Eng. Struct*., **123**, 124-140. https://doi.org/10.1016/j.engstruct.2015.05.012

Ataei, A., Bradford, M.A. and Valipour, H.R. (2016b), “Finite element analysis of HSS semi-rigid composite joints with precast concrete slabs and demountable bolted shear connectors”, *Finite Elem. Anal. Des*., **122**, 16-38. https://doi.org/10.1016/j.finel.2016.08.003

Ataei, A., Bradford, M.A. and Liu, X. (2017), “Computational modelling of the moment-rotation relationship for deconstructable flush end plate beam-to-column composite joints”, *J. Constr. Steel Res*., **129**, 75-92. https://doi.org/10.1016/j.jcsr.2016.11.007

Ataei, A. and Bradford, M.A. (2016), “Numerical study of deconstructable flush end plate composite joints to concrete-filled steel tubular columns”, *Structures*, **8**, 130-143. https://doi.org/10.1016/j.istruc.2016.09.009

Elremaily, A. and Azizinamini, A. (2001), “Experimental behavior of steel beam to CFT column connections”, *J. Constr. Steel Res*., **57**(10), 1099-1119. https://doi.org/10.1016/S0143-974X(01)00025-6

Eom, S.S., Vu, Q.V., Choi, J.H., Park, H.H. and Kim, S.E. (2019), “Flexural behavior of concrete-filled double skin steel tubes with a joint”, *J. Constr. Steel Res*., **155**, 260-272. https://doi.org/10.1016/j.jcsr.2018.12.012

Esfandyary, R., Razzaghi, M.S. and Eslami, A. (2015), “A parametric investigation on the hysteretic behaviour of CFT column to steel beam connections”, *Struct. Eng. Mech., Int. J.*, **55**(1), 205-228. https://doi.org/10.12989/sem.2015.55.1.205

Eurocode 2: Design of concrete structures- Part 1-1 (2004), EUROPEAN COMMITIEE FOR STANDARDIZATION.

Han, L.H., Tao, Z., Huang, H. and Zhao, X.L. (2004), “Concrete-filled double skin (SHS outer and CHS inner) steel tubular beam-columns”, *Thin-Wall. Struct*., **42**(9), 1329-1355. https://doi.org/10.1016/j.tws.2004.03.017

Han, T.H., Stallings, J.M. and Kang, Y.J. (2010), “Nonlinear concrete model for double-skinned composite tubular columns”, *Constr. Build. Mater*., **24**(12), 2542-2553. https://doi.org/10.1016/j.conbuildmat.2010.06.001

Hassan, M.M., Ramadan, H.M., Naeem, M. and Mourad, S.A. (2014), “Behavior of gusset plate-T0-CCFT connections with different configurations”, *Steel Compos. Struct*., *Int. J.*, **17**(5), 735-751. https://doi.org/10.12989/scs.2014.17.5.735

Hassan, M.M., Mahmoud, A.A. and Serror, M.H. (2016), “Behavior of concrete-filled double skin steel tube beam-columns”, *Steel Compos. Struct., Int. J*., **22**(5), 1141-1162. https://doi.org/10.12989/scs.2016.22.5.1141

Jordão, S., Simões da Silva, L. and Simões, R. (2014), “Design formulation analysis for high strength steel welded beam-to-column joints", *Eng. Struct*., **70**, 63-81. https://doi.org/10.1016/j.engstruct.2014.02.028

Kim, S.E. and Nguyen, H.T. (2010), "Finite element modeling and analysis of a hybrid steel-PSC beam connection", *Eng. Struct*., **32**(9), 2557-2569. https://doi.org/10.1016/j.engstruct.2010.04.029

Kim, S.E. and Nguyen, H.T. (2012), "Evaluation of the connection efficiency of hybrid steel-concrete girder using finite element approach", *Int. J. Mech. Sci*., **61**(1), 8-23. https://doi.org/10.1016/j.ijmecsci.2012.04.008

Korean Buidling Code (2016), Architectural Institute of Korea, Korea.

Korean Design Standard (2017), Korean Industrial Standards, Seoul, Korea.

Korean Standard KS F 2405 (2010), Korean Standards Association, Korea.

Korean Standard KS D 3515:2014 (2014), Korean Standards Association, Seoul, Korea.

Korean Structural Concrete Design Code (2012), Korean Concrete Institute, Korea.

Li, D., Wang, J., Uy, B., Aslani, F. and Patel, V. (2018), "Analysis and design of demountable circular CFST column-base connections", *Steel Compos. Struct., Int. J*., **28**(5), 559-571. https://doi.org/10.12989/scs.2018.28.5.559

Loh, H.Y., Uy, B. and Bradford, M.A. (2006), "The effects of partial shear connection in composite flush end plate joints. Part I-Experimental study", *J. Constr. Steel Res*., **62**(4), 378-390. https://doi.org/10.1016/j.jcsr.2005.07.012

Moon, J., Roeder, C.W., Lehman, D.E. and Lee, H.E. (2012), "Analytical modeling of bending of circular concrete-filled steel tubes", *Eng. Struct*., **42**, 349-361. https://doi.org/10.1016/j.engstruct.2012.04.028

Tao, Z. and Han, L.H. (2006), "Behaviour of concrete-filled double skin rectangular steel tubular beam-columns", *J. Constr. Steel Res*., **62**(7), 631-646. https://doi.org/10.1016/j.jcsr.2005.11.008

Thai, H.T. and Uy, B. (2015), "Finite element modelling of blind bolted composite joints", *J. Constr. Steel Res*., **112**, 339-353. https://doi.org/10.1016/j.jcsr.2015.05.011

Thai, H.T., Uy, B. and Aslani, F. (2017), "Behaviour of bolted endplate composite joints to square and circular CFST columns", *J. Constr. Steel Res*., **131**, 68-82. https://doi.org/10.1016/j.jcsr.2016.12.022

Thomas, J. and Sandeep, T.N. (2018), "Experimental study on circular CFST short columns with intermittently welded stiffeners", *Steel Compos. Struct., Int. J*., **29**(5), 659-667. https://doi.org/10.12989/scs.2018.29.5.659

Tong, L., Huang, X., Zhou, F. and Chen, Y. (2016), "Experimental and numerical investigations on extremely-low-cycle fatigue fracture behavior of steel welded joints", *J. Constr. Steel Res*., **119**, 98-112. https://doi.org/10.1016/j.jcsr.2015.12.015

Vu, Q.V., Thai, D.K. and Kim, S.E. (2018), "Effect of intermediate diaphragms on the load-carrying capacity of steel-concrete composite box girder bridges", *Thin-Wall. Struct*., **122**, 230-241. https://doi.org/10.1016/j.tws.2017.10.024

Wang, J.F., Han, L.H. and Uy, B. (2009a), "Behaviour of flush end plate joints to concrete-filled steel tubular columns", *J. Constr. Steel Res*., **65**(4), 925-939. https://doi.org/10.1016/j.jcsr.2008.10.010

Wang, J.F., Han, L.H. and Uy, B. (2009b), "Hysteretic behaviour of flush end plate joints to concrete-filled steel tubular columns", *J. Constr. Steel Res*., **65**(8-9), 1644-1663. https://doi.org/10.1016/j.jcsr.2008.12.008

Wang, J., Uy, B. and Li, D. (2018), "Analysis of demountable steel and composite frames with semi-rigid bolted joints", *Steel Compos. Struct., Int. J*., **28**(3), 363-380. https://doi.org/10.12989/scs.2018.28.3.363

Waqas, R., Uy, B. and Thai, H.T. (2019), "Experimental and numerical behaviour of blind bolted flush endplate composite connections", *J. Constr. Steel Res*., **153**, 179-195. https://doi.org/10.1016/j.jcsr.2018.10.012

Yang, C.M. and Kim, Y.M. (2007), "Cyclic behavior of bolted and welded beam-to-column joints", *Int. J. Mech. Sci*., **49**(5), 635-649. https://doi.org/10.1016/j.ijmecsci.2006.09.022

Yang, J., Sheehan, T., Dai, X.H. and Lam, D. (2015), "Experimental study of beam to concrete-filled elliptical steel tubular column connections", *Thin-Wall. Struct*., **95**, 16-23. https://doi.org/10.1016/j.tws.2015.06.009

Yuan, F., Chen, M. and Huang, H. (2019), "Square CFST columns under cyclic load and acid rain attack: Experiments", *Steel Compos. Struct*., *Int. J*., **30**(2), 171-183. https://doi.org/10.12989/scs.2019.30.2.171

BU

Notation

b_{sbb}	Width of steel box beam
h_{sbb}	Depth of steel box beam
E_s	Elastic modulus of steel
f_{ck}	Cylinder compressive strength of concrete
f'_{c1}	Compressive strength of concrete slab
f'_{c2}	Compressive strength of concrete infill
f_{tk}	Tensile strength of concrete
F_y	Yield strength of steel
F_u	Ultimate strength of steel
t_f	Flange thickness of steel box beam
t_w	Web thickness of steel box beam
ε_y	Yield strain of steel
ε_u	Ultimate strain of steel
ε_c	Strain of the peak compressive stress f_{ck}